The Use of Digital Twins in Inverter-based DERs to Improve Nanogrid Fault Recovery

Andrew Eggebeen dept. of Computer Science Milwaukee, WI, USA eggebee6@uwm.edu

Mark Vygoder dept. of Electrical Engineering University of Wisconsin - Milwaukee University of Wisconsin - Milwaukee Milwaukee, WI, USA mvygoder@uwm.edu

Giovanna Oriti dept. of Electrical and Computer Engineering Naval Postgraduate School Monterey, CA, USA https://orcid.org/0000-0001-8520-6590

Jacob Gudex dept. of Electrical Engineering University of Wisconsin - Milwaukee Milwaukee, WI, USA jdgudex@uwm.edu

Alexander L. Julian Consultant Seaside, CA, USA https://orcid.org/0009-0008-3997-0422

Robert M. Cuzner dept. of Electrical Engineering University of Wisconsin - Milwaukee Milwaukee, WI, USA cuzner@uwm.edu

Abstract-Nanogrids provide a redundant mode of operation when the grid power fails. Nanogrids use data communication networks to coordinate power and energy between distributed energy resources (DERs). Under the corner-case of simultaneous communication failure and electrical faults, it can be difficult for the energy storage system with grid-forming/grid-following capability to select the correct operational mode. This paper proposes the use of a digital twin to assist in minimizing the degradation on the nanogrid caused by loss of communication during islanded operation under electrical fault conditions. The structure of the digital twin is proposed, and the construction of a virtual twin is presented. The error vector produced by the difference between the physical twin and virtual twin is demonstrated in various fault conditions. Lastly, the paper presents a discussion of how the error vector could be used to make inferences about the nanogrid state and to choose actions during off-nominal communication.

Index Terms-Digital Twin, Microgrid, Nanogrid, Resilience, Distributed Energy Resources, Machine Learning

I. INTRODUCTION

Larger industrial facilities can feature complex electrical power systems (EPS) which can be spread out over a large geographical area. Within the industrial facility, portions of the EPS can be segmented into zones. The zones are identified by geographically separated regions of critical loads. Load criticality is tied to the operation of the facility, e.g. expensive and complex manufacturing processes, security or safety systems, water/waste water treatment, etc.

Microgrids provide additional distributed energy resources (DERs) and additional modes of operations in the presence of electrical grid failure, which can increase the EPS' resilience [1]-[3]. If the whole facility operating in islanded mode is a microgrid, then a smaller portion of the EPS operating in islanded mode is a nanogrid [4], [5]. The larger microgrid can be built up of smaller nanogrids with the nanogrids located at

This work was partially sponsored by the NAVFAC Naval Shore Energy Technology Transition and Integration (NSETTI) program and by the National Science Foundation, Grant No. 1439700.

the facility critical loads. If the critical loads are geographically separated, then the EPS can be divided into zones, supported by nanogrids, or zonal nanogrids. The zonal nanogrid proves an additional redundant mode of operation should the larger microgrid fail [4]. Nanogrids also offer a cost-effective way for larger facilities to improve the resilience of their EPS by building up smaller systems one at a time compared to one large microgrid.

When the nanogrid is the sole remaining source of power and energy, the DERs with the nanogrid, nanogrid controllers, and switchgear/automatic transfer switches (ATS) must coordinate efficiently and effectively to deliver power/energy to the right place at the right time. This coordination requires an exchange of data, making the nanogrid a cyber-physical system reliant on a data communication network. Thus, the impact of nominal and off-nominal communication should be assessed under nominal and off-nominal electrical conditions, where simultaneous communication and electrical faults pose the extreme corner case for which solutions must be designed.

Fig. 1 shows a case-study for a nanogrid built with commercial-off-the-shelf (COTS) equipment. The nanogrid is designed to support the critical water treatment plant of an industrial facility. The nanogrid is comprized of two distribution voltage levels: one at 13.8 kV medium voltage, and one at 480 V low voltage. The medium voltage switchgear serves as the interface of the nanogrid to the rest of the EPS. The low voltage switchgear serves as the interface for the DERs and loads.

The nanogrid is operating in islanded-mode with the diesel genset enabled. The genset is supplying the loads connected to the nanogrid and is charging the battery energy storage system (BESS).

Proper coordination between the protection settings in the distribution equipment and the DER low-voltage ride-through (LVRT) settings in the power conversion equipment is needed to ensure the maximum number of DERs will ride through the

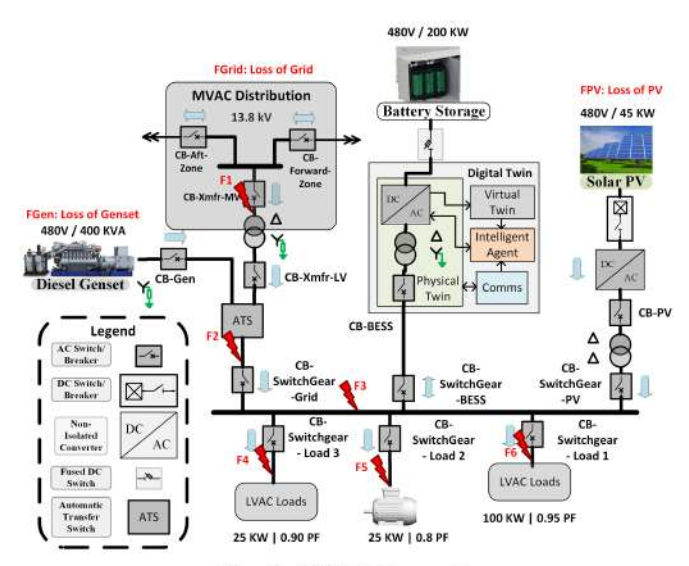


Fig. 1: COTS Nanogrid.

fault [6]. Assuming IEEE Std. 1547-2018 Category III ridethrough [7] is applied to the BESS, the BESS converter must know under which fault conditions it should disconnect, perform momentary cessation, or switch to grid-forming/voltagecontrol mode.

To demonstrate this point, Fig. 2 and Fig. 3 show line-toline faults between phase A and B (LLab) at fault location 4 (F4) and 2 (F2), respectively, as shown in Fig. 1. For the downstream fault at F4, the BESS enters momentary cessation, the genset contributes fault current, the circuit breaker (CB)-SwitchGear-Load-3 opens, and the BESS resumes operation. For the upstream fault at F2, the BESS enters momentary cessation, CB-Gen trips, and after 1 second the BESS switches to grid-forming. This provides fault current for the directional overcurrent relay at CB-Switchgear-Grid.

This example only shows a LLab fault in two locations under one configuration. However, other configurations, such as genset + BESS + PV, BESS + PV, Grid + BESS + PV, etc., must also be taken into account. One set of ride-through settings may not be optimal for all possible configurations, fault types, and fault locations.

Knowledge of the neighboring breakers and DERs states through a high-speed communication network would simplify the complexity of proper ride-through operation. However, if the communication experiences degradation or failure (equipment malfunction, cyber-attack, etc.), making the proper ride-through decision for the BESS will be significantly more difficult.

Several works have demonstrated detrimental effects on EPS caused by off-nominal communications [8]–[10], but to the best of the authors' knowledge, no previous work is available in literature addressing nanogrid resilience during off-nominal data communication in the midst of an electrical fault. We propose the use of digital twins (DTs) to minimize the impact of simultaneous electrical and communication faults,

and to improve the systems recovery via proper ride-through performance of the BESS.

During off-nominal communications, the BESS must be able to estimate the state of the nanogrid without being able to communicate with other devices. The use of a DT will allow the BESS to extract physics-based information from its measurements which can be used to gain insights and help determine the correct mode of operation the BESS converter should be in.

A. Literature Review of Digital Twins

A DT for smart grids is presented in [11]. Automatic Network Guardian for Electrical (ANGEL) systems monitors a smart grid using SCADA and other communication techniques to gather measurements in real-time. These measurements are used by a simulation of the grid, which is also run in real-time. By comparing the received measurements to the measurements predicted by the DT simulation, anomalies including electrical faults and false data injection can be detected. The authors note the need for real-time communication, thus identifying communication delays or failures as a potential weakness.

Artificial neural networks (ANN) are employed in [12] to locate faults in a smart grid. Measurements from smart meters in the grid are sent across a communication network and used as inputs to the ANN. The ANN outputs are used to detect and locate faults. Use of the ANN aids in the analysis of a fault by simplifying the transient state estimation (TSE) equation, allowing the TSE to be solved only for the faulted parts of the system rather than the entire system. The authors also note the need for real-time communication.

Use of a deep learning convolutional neural network (CNN) for smart grid anomaly detection is presented in [13]. The CNN is demonstrated on the IEEE 9-bus model and the IEEE 39-bus model. Three-phase voltages from each bus are used as inputs to the CNN. The CNN detects faults and estimates which bus in the model has been faulted.

A DT for a battery system is presented in [14]. A simulation of the battery system was created, and a rule-based system was used to detect anomalies in the battery state of charge (SoC). Anomalies were detected by a divergence between the predicted SoC and actual SoC. The authors identified the importance of an accurate model of the system and noted the need for timely communication between the battery system and the simulation. A related work [15] improves the battery model by training a CNN to predict the battery system response.

A medium voltage (MV) to low voltage (LV) distribution transformer DT is given in [16]. Voltage and current measurements are taken on the LV side of the transformer. A simplified model of the transformer circuit is used to estimate the voltages and currents on the MV side of the transformer given the LV side measurements. The authors use a statistical comparison and a frequency analysis of the model output, testing its predictions against data recorded from a real transformer.

In [17], a nonlinear autoregressive network with exogenous inputs (NARX) is used to model the dynamics of a power converter. The NARX model is used to predict inductor current and capacitor voltage for the converter given the converter's duty cycle, input voltage, and load current. Once trained, the NARX model can be run in real-time alongside the converter to predict the expected converter measurements. The model is validated by testing its response in both the time domain and the frequency domain.

A DT is recommended for self-security of inverters in [18]. The DT contains knowledge of IEEE Std. 1547-2018 requirements and of the safe operating region and dynamic response of the inverter. Commands to change the PQ setpoints can be sent to the inverter, and the DT will compare these setpoints to its knowledge of the inverter and the current state of the system. If the PQ setpoints would cause a problem, the DT rejects the setpoints. Rejecting invalid PQ setpoints keeps the inverter in a safe state, protecting against both malicious and unintentionally dangerous commands.

A DT for a photovoltaic energy conversion unit (PVECU) is demonstrated in [19]. The DT contains a state-space model of the converter to model the inductor current and output capacitor voltage. The DT also contains knowledge of the maximum power point (MPP) current and voltage of the PV panel. Using measurements of the inductor current, capacitor voltage, PV irradiance levels, and PV panel temperature, the DT predicts what the measurements will be at the next timestep. An error vector at a given timestep is calculated as the difference between the predicted measurements and the actual measurements at that timestep. Tolerance levels are set for each dimension of the error vector, and the DT signals a fault if any of the tolerances are exceeded. An inner-product calculation is used to compare the trajectory of the error vector to a library of pre-calculated fault vectors, using the result to predict which type of fault (if any) is occurring.

A probabilistic approach to analyzing an error vector is given in [20]. The state-space model is formulated where the coefficient matrices are treated as stochastic processes. The error vector is calculated similar to [19], but the use of polynomial chaos expansion (PCE) allows the tolerance levels of the error vector to be varied probabilistically. This approach can model random effects of the physical device, such as circuit components being manufactured within a random tolerance of their rated value, thus allowing the DT to detect faults while tolerating the expected variances in its physical counterpart.

B. Paper contributions and organization

The contributions of this paper include the following:

- A novel DT structure including the physical twin, virtual twin, intelligent agent, and data communication
- Description of a BESS physical twin and derivation of a state-space model for the BESS virtual twin
- 3) Formulation of the virtual twin error vector

The paper is organized as follows: Section II proposes a novel structure for the DT. Section III formulates the virtual

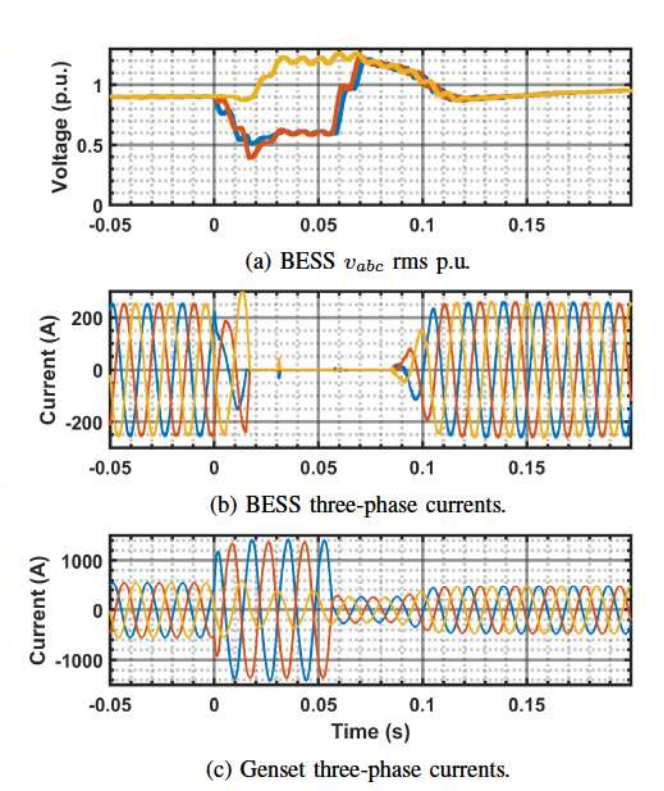


Fig. 2: Line-to-line fault between phases A and B at F4.

twin for the BESS. Section IV presents simulation results of the error vector and Section V draws some conclusions.

II. DIGITAL TWINS

A. Overview

Based on the review of DT literature, the proposed DT design consists of four layers:

- Physical Twin the physical device itself
- Virtual Twin a real-time, physics-based simulation of the physical twin
- Intelligent Agent a model of the learning and decision making processes
- Data Communications data exchange with other devices, services, or human operators

One of the goals of the DT is to perform actions which are most likely to maximize a utility function. The physical twin will have sensors to measure its present state (e.g. voltages, currents) and actuators to affect its future state (e.g. digital control signals and gate signals). The virtual twin is an upto-date digital model of the physical twin and is used to provide physics-based information about the physical twin. Data communication allows the DT to exchange information with other devices or humans. The intelligent agent, or simply the *agent*, of the DT follows a *sense-decide-act* loop [21], [22]. This loop consists of three stages:

- Sense take sensor measurements from the physical twin
- Decide evaluate possible actions and choose an action to be performed

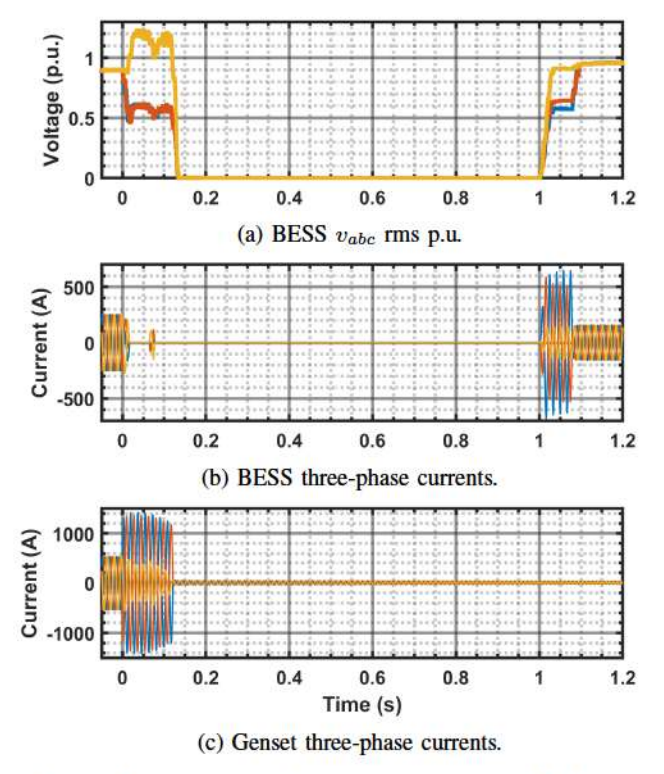


Fig. 3: Line-to-line fault between phases A and B at F2.

 Act - perform the chosen action by configuring the physical twin actuators

This loop is performed continuously during the DT's operation. During each repetition of this loop, the following steps take place:

- Read the physical twin state x_t from the physical twin sensors
- 2) Calculate and store the predicted state $\hat{\mathbf{x}}_{t+1}$ for the next timestep
- 3) Calculate the error vector ϵ_t for the current timestep
- Use the error vector and other relevant information to choose an action
- Configure the physical twin actuators according to the action

B. Virtual Twin

The virtual twin is a real-time digital representation of the physical twin [5], [23], [24]. The virtual twin must be:

- · Physics based
- Real-time capable
- · Driven by physical twin sensor measurements

The virtual twin's understanding of the physical model can be used to monitor and protect the physical twin. Using its understanding of the physical twin dynamics, a virtual twin can monitor the health of the physical twin [11], [12], [19], [20], [25], analyze its behavior and its interaction with the environment [14], [15], [19], [20], and prevent it from being placed in a dangerous state [18].

The virtual twin provides physics-based information to the agent. The virtual twin uses the physical twin sensor measurements along with other physical information, such as actuator configuration, to make a prediction about the values of the next sensor measurements which will be taken.

Several methods of creating a virtual twin model have been explored. The physical twin model can be viewed as a blackbox (completely unknown), gray-box (partially known), or white-box (fully known) [17], [26]. A gray-box approach is taken in [17], where the details of the converter are learned from recorded measurements in a test environment. Statespace modelling is a white-box approach and is used to create the virtual twins in [19], [20].

A state-space model is a set of differential equations which represent the dynamics of the physical twin. A simple state-space model is given in (1), where x is the state vector, \dot{x} is the change in state vector, and u is the system input vector. The virtual twin prediction function uses this state-space model along with an integration method such as Forward Euler, i.e. (2), to estimate what the state of the physical twin will be at the next timestep. Equation (3) shows the virtual twin prediction function as a combination of (1) and (2). Both x_t and u_t are measured from the physical twin on each timestep, so (3) only needs to predict one timestep ahead.

$$\dot{x}_t = \frac{d}{dt}x_t = A \cdot x_t + B \cdot u_t \tag{1}$$

$$\hat{x}_{t+1} = x_t + \Delta t \cdot \frac{d}{dt} x_t \tag{2}$$

$$\hat{x}_{t+1} = (I + \Delta t \cdot A) \cdot x_t + \Delta t \cdot B \cdot u_t \tag{3}$$

An error vector is constructed on each timestep, where the error vector is the difference between the measurements taken on the timestep and the measurements predicted from the previous timestep. Equation (4) shows the calculation of the error vector, where \hat{x}_t is the prediction from the previous timestep.

$$\epsilon_t = \hat{x}_t - x_t \tag{4}$$

The error vector can be used to quantify the effects acting on the physical twin which are not captured in the virtual twin model. For example, an electrical fault in the nanogrid will affect the physical twin measurements, but the virtual twin does not model the dynamics and states of the interfacing nanogrid, so the effects of the fault will be captured in the error vector.

Error vectors can be analyzed by the agent to make inferences about outside effects acting on the physical twin. The output of the machine learning (ML) model could be used to decide on an action, such as choosing the proper IEEE std. 1547-2018 ride-through action or changing from grid-following to grid-forming mode.

III. DIGITAL TWIN FOR A BESS VSC

Fig. 4 shows an example DT for the voltage source converter (VSC) of a battery energy storage system (BESS). Fig. 5 shows the VSC topology being modelled by the virtual twin.

$$x = \begin{bmatrix} i_{Lfa} & i_{Lfb} & i_{Lfc} & v_{Cfa} & v_{Cfb} & v_{Cfc} & i_{Loa} & i_{Lob} & i_{Loc} \end{bmatrix}^T$$

$$(5)$$

$$u = \begin{bmatrix} v_{DC} & v_{DC} & v_{DC} & v_{ga} & v_{gb} & v_{gc} \end{bmatrix}^T$$

$$(6)$$

$$A = \begin{bmatrix} \frac{-R_f}{L_f} & 0 & 0 & \frac{-2}{3L_f} & \frac{1}{3L_f} & \frac{1}{3L_f} & \frac{R_f}{L_f} & 0 & 0\\ 0 & \frac{-R_f}{L_f} & 0 & \frac{1}{3L_f} & \frac{1}{3L_f} & \frac{1}{3L_f} & 0 & \frac{R_f}{L_f} & 0\\ 0 & 0 & \frac{-R_f}{L_f} & \frac{1}{3L_f} & \frac{1}{3L_f} & \frac{-2}{3L_f} & 0 & 0 & \frac{R_f}{L_f}\\ \frac{1}{C_f} & 0 & 0 & 0 & 0 & 0 & \frac{-1}{C_f} & 0 & 0\\ 0 & \frac{1}{C_f} & 0 & 0 & 0 & 0 & \frac{-1}{C_f} & 0 & 0\\ 0 & 0 & \frac{1}{C_f} & 0 & 0 & 0 & 0 & \frac{-1}{C_f} & 0\\ 0 & 0 & \frac{1}{L_f} & 0 & 0 & \frac{-(R_f + R_o)}{L_f} & 0 & 0 & 0\\ \frac{R_f}{L_f} & 0 & 0 & \frac{1}{L_f} & 0 & 0 & \frac{-(R_f + R_o)}{L_f} & 0\\ 0 & \frac{R_f}{L_f} & 0 & 0 & \frac{1}{L_f} & 0 & 0 & \frac{-(R_f + R_o)}{L_f} & 0\\ 0 & 0 & \frac{R_f}{L_f} & 0 & 0 & \frac{1}{L_f} & 0 & 0 & \frac{-(R_f + R_o)}{L_f} \end{bmatrix}$$

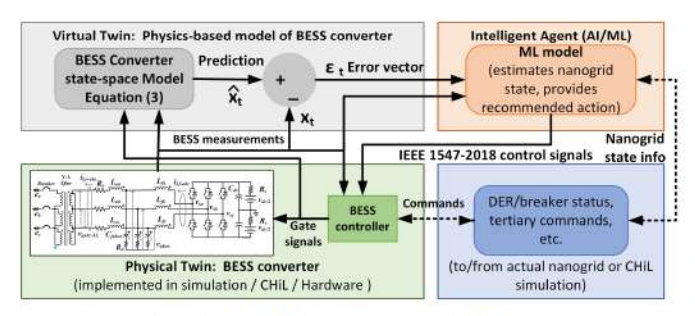


Fig. 4: Block Diagram of BESS DT

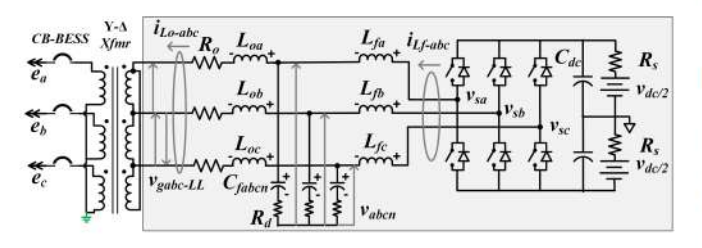


Fig. 5: Virtual twin model of BESS VSC

The BESS VSC includes an LCL filter with passive damping, an interfacing Y- Δ transformer, and an output circuit breaker (labeled as CB-BESS in Fig. 1). The transformer is grounded on the Y side. The virtual twin only models the topology highlighted in the gray box in Fig. 5.

The physical twin has sensors to take the following measurements:

- Filter inductor currents i_{Lf-abc}
- Filter capacitor voltages v_{Cf-abc}
- Output inductor currents i_{Lo-abc}
- DC source voltage v_{DC}
- Grid connection voltages v_{q-abc}

These measurements are noted in Fig. 5. In addition, the state of the converter gate drives S_a , S_b , and S_c is known on each timestep.

A. Virtual Twin model for BESS VSC

The virtual twin prediction function is created as described in (3). The state vector x_t consists of inductor currents and capacitor voltages from the LCL filter, i_{Lf-abc} , v_{Cf-abc} , and i_{Lo-abc} , as shown in (5). The input vector u_t consists of v_{DC} and v_{g-abc} , as shown in (6). The matrices A and B in (3) are derived from the converter and filter topology, as shown in (7) and (8), respectively.

The switch states S_a , S_b , and S_c (S_a , S_b , S_c ϵ $\{-1,1\}$) are part of the B matrix, where S_a , S_b , and S_c represent either the upper switch (1) or lower switch (-1) being on for phase leg A, B, or C, respectively. The switch state is multiplied by $v_{DC}/2$ to represent the voltages at the midpoints of each phase leg (v_{sa} , v_{sb} , and v_{sc} in Fig. 5).

On each timestep, the state vector x_t and input vector u_t is created by sampling each of the respective physical twin

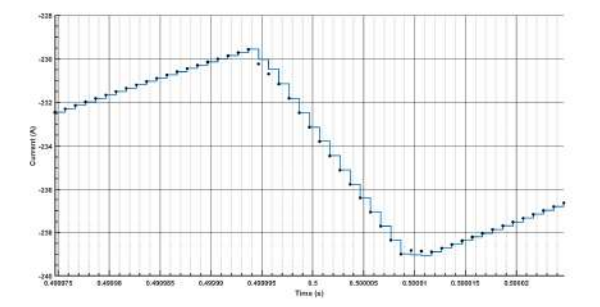


Fig. 6: L_o phase A measured current (line) and predicted currents (dots)

sensors. The B matrix is updated with switch states S_a , S_b , and S_c . The virtual twin creates the prediction for the next timestep, and the error vector for the current timestep is calculated and stored for processing.

It is worth noting that often times in the derivation of state-space model for 3-phase VSC with LCL filters, a single-phase equivalent circuit is used. However, this does not capture the constraint that the sum of current of the inverter must comply with Kirchhoff's current law (KCL), i.e., $i_{Lfa}+i_{Lfb}+i_{Lfc}=0$. Thus, the single-phase equivalent circuit would not capture the effects of imbalances within the state-space model. To solve for the state-space model while capturing the KCL constraint, the VSC line-to-line output voltages are used which accounts for the cross-coupling terms in the three-by-three block $a_{41}-a_{63}$ in matrix A and in $b_{11}-b_{33}$ in matrix B.

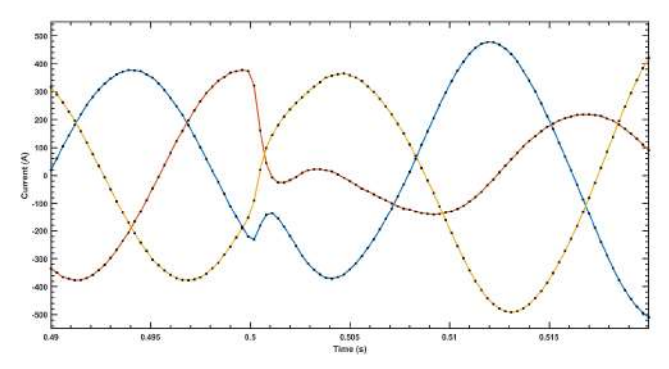
It is also worth noting that this virtual twin model does not include BESS controller parameters, it only models the physics of the converter. It is not tied to a specific controller or control algorithm, thus making it an adaptable and generic approach to creating a virtual twin.

IV. SIMULATION RESULTS

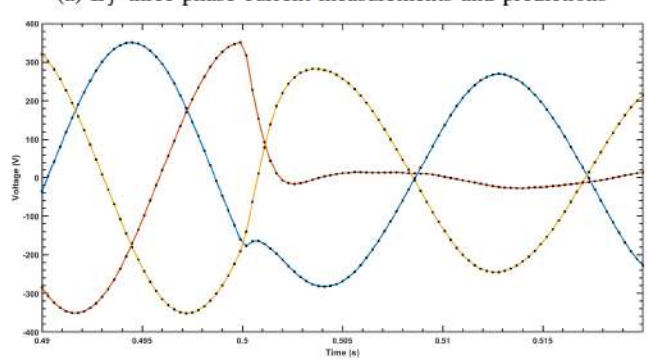
Simulations of the nanogrid in Fig. 1 were performed in Matlab/Simulink, including simulations for fault types F2 and F4. In both simulations, the faults occur at time 0.5 seconds. Since the error vector for the BESS DT is 9-dimensional, it cannot be fully plotted on a single diagram. Instead, plots of the error vector magnitudes (calculated with the L^2 norm) can be used to illustrate some of the error vector patterns. Error vector analysis is not subject to this limitation and may take full advantage of all 9 dimensions.

Fig. 6 shows a plot of the measured L_o current from phase A with its predicted measurements overlaid as dots. Figs. 7a, 7b, and 7c show the three-phase measurements and predictions from L_f , C_f , and L_o , respectively. These plots show that the state-space model of the virtual twin follows the behavior of the BESS physical twin with a high degree of accuracy.

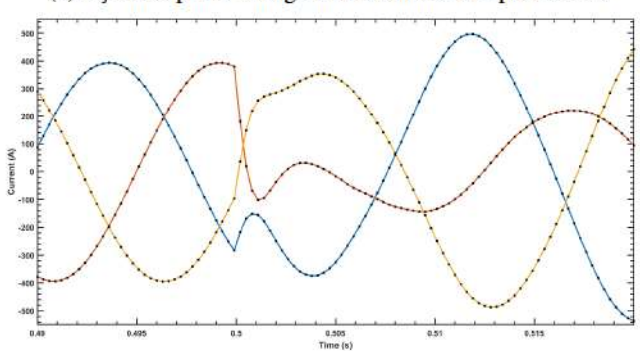
Figs. 8 and 9 include plots of BESS DT measurements and of error vectors created from the v_{Cf} and i_{Lo} components of the overall error vector \hat{x} . Figs. 8a and 8b show the measurements and error vector magnitudes for C_f and Figs.



(a) L_f three-phase current measurements and predictions



(b) C_f three-phase voltage measurements and predictions



(c) L_o three-phase current measurements and predictions

Fig. 7: BESS DT measurements and predictions

8c and 8d show the measurements and error vector magnitudes for L_o during fault F2. Similar plots are provided in Fig. 9 to show the values during fault F4.

The error vectors can be used to quickly detect a divergence from expected operation, for example in Figs. 8d and 9d by the sudden increase in inductor current error vector magnitude at fault inception similar to [19], [20]. The error vectors could also be used to identify the cause of a divergence, for example by the patterns in capacitor voltage similar to [12], [13]. ML models can be trained to learn the subtle and complex features of the error vectors in different situations (e.g. F2 vs. F4). For example, the agent could include a trained ML model to recognize features in the error vectors, similar to the ANN in [12] or CNN's in [13], [15].

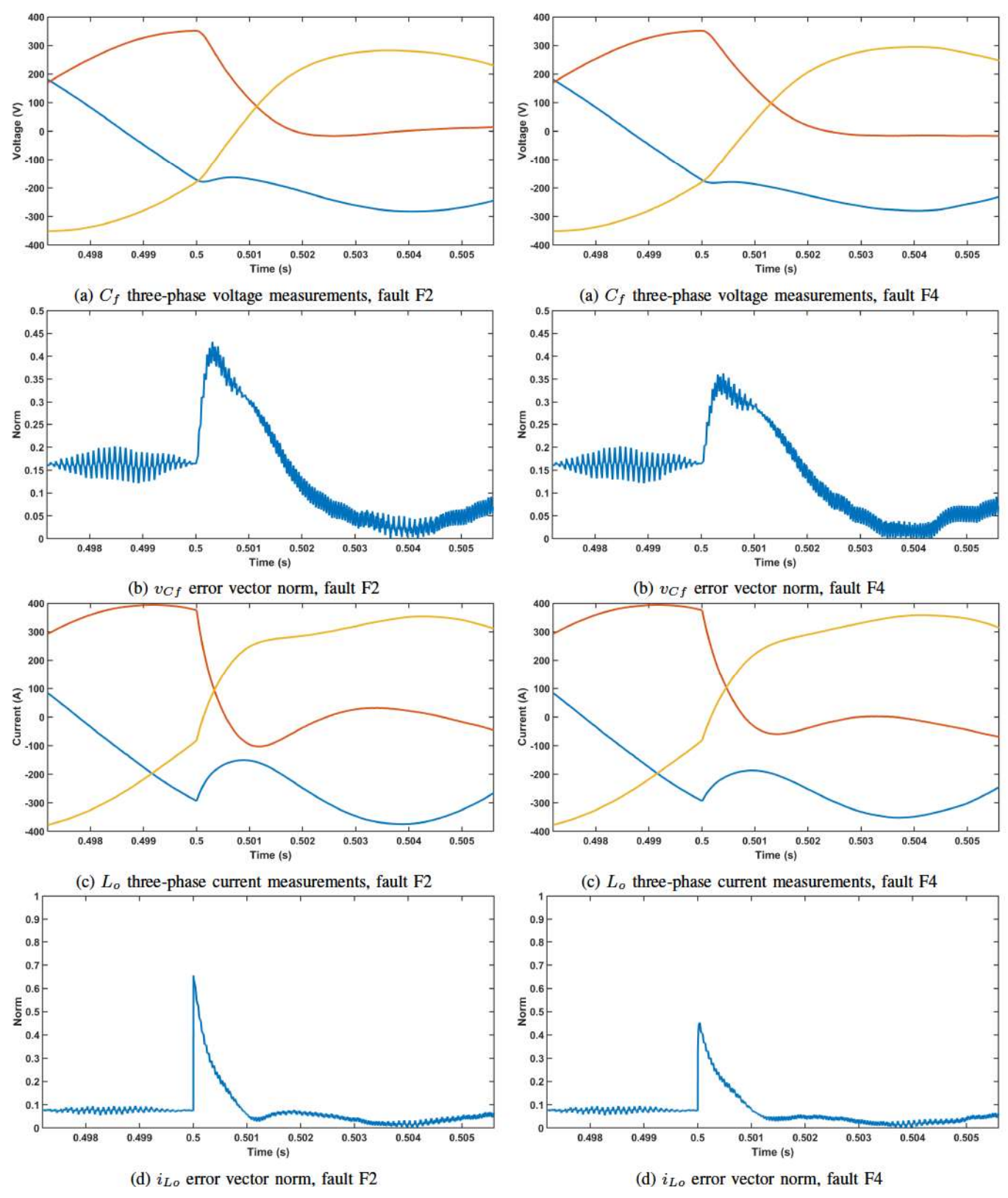


Fig. 8: BESS DT \mathcal{C}_f and \mathcal{L}_o during fault F2

Fig. 9: BESS DT C_f and L_o during fault F4

During nominal data communications, the BESS DT will be receiving information about the nanogrid state from the communication network, including commands from a centralized nanogrid controller. The received data can be paired with the error vectors being recorded by the DT, and a ML model could be trained to recognize nanogrid states from error vectors alone. Using the error vectors in this fashion could allow the DT to recognize the nanogrid state and make the appropriate IEEE Std. 1547-2018 ride-through action without the need for active communication with a centralized nanogrid controller.

V. CONCLUSION

This paper describes the creation of a virtual twin for a BESS DT. Use of the virtual twin provides physics-based information about its physical twin in the form of an error vector. This error vector can be used as a feature for detecting and identifying events in the nanogrid such as electrical faults. The physical twin for a BESS was identified and a state-space model was developed to calculate the virtual twin error vector. Simulations were conducted of a COTS nanogrid, and the error vector was demonstrated under fault conditions. The approach to creating the BESS virtual twin is generic, straightforward, and can be applied for the development of other DERs or nanogrid digital twins.

REFERENCES

- R. E. Giachetti, D. L. Van Bossuyt, W. W. Anderson, and G. Oriti, "Resilience and cost trade space for microgrids on islands," *IEEE Systems Journal*, vol. 16, no. 3, pp. 3939–3949, 2021.
 P. Siritoglou, G. Oriti, and D. L. Van Bossuyt, "Distributed energy-
- [2] P. Siritoglou, G. Oriti, and D. L. Van Bossuyt, "Distributed energy-resource design method to improve energy security in critical facilities," *Energies*, vol. 14, no. 10, p. 2773, 2021.
- [3] N. Anglani, G. Oriti, R. Fish, and D. L. Van Bossuyt, "Design and optimization strategy to size resilient stand-alone hybrid microgrids in various climatic conditions," *IEEE Open Journal of Industry Applica*tions, vol. 3, pp. 237–246, 2022.
- [4] A. Kain, D. L. Van Bossuyt, and A. Pollman, "Investigation of nanogrids for improved navy installation energy resilience," *Applied Sciences*, vol. 11, no. 9, p. 4298, 2021.
- [5] N. Bazmohammadi, A. Madary, J. C. Vasquez, H. B. Mohammadi, B. Khan, Y. Wu, and J. M. Guerrero, "Microgrid digital twins: Concepts, applications, and future trends," *IEEE Access*, vol. 10, pp. 2284–2302, 2021.
- [6] M. Vygoder, F. Banihashemi, J. Gudex, R. M. Cuzner, and G. Oriti, "Coordination of protection and ride-through settings for islanded facility microgrids," in 2021 IEEE Energy Conversion Congress and Exposition (ECCE). IEEE, 2021, pp. 1095–1102.
- [7] "IEEE standard for interconnection and interoperability of distributed energy resources with associated electric power systems interfaces," IEEE Std 1547-2018, pp. 1–138, 2018.
- [8] X. Lou, C. Tran, R. Tan, D. K. Yau, Z. T. Kalbarczyk, A. K. Banerjee, and P. Ganesh, "Assessing and mitigating impact of time delay attack: Case studies for power grid controls," *IEEE Journal on Selected Areas in Communications*, vol. 38, no. 1, pp. 141–155, 2019.
- [9] A. Saad, S. Faddel, T. Youssef, and O. A. Mohammed, "On the implementation of IoT-based digital twin for networked microgrids resiliency against cyber attacks," *IEEE transactions on smart grid*, vol. 11, no. 6, pp. 5138–5150, 2020.
- [10] R. Heydari, Y. Khayat, A. Amiri, T. Dragicevic, Q. Shafiee, P. Popovski, and F. Blaabjerg, "Robust high-rate secondary control of microgrids with mitigation of communication impairments," *IEEE Transactions on Proper Floritories*, vol. 35, no. 11, pp. 12486-12496, 2020.
- Power Electronics, vol. 35, no. 11, pp. 12486–12496, 2020.
 [11] W. Danilczyk, Y. Sun, and H. He, "ANGEL: An intelligent digital twin framework for microgrid security," in 2019 North American power symposium (NAPS). IEEE, 2019, pp. 1–6.

- [12] N. Tzanis, N. Andriopoulos, A. Magklaras, E. Mylonas, M. Birbas, and A. Birbas, "A hybrid cyber physical digital twin approach for smart grid fault prediction," in 2020 IEEE Conference on Industrial Cyberphysical Systems (ICPS), vol. 1. IEEE, 2020, pp. 393–397.
- [13] W. Danilczyk, Y. L. Sun, and H. He, "Smart grid anomaly detection using a deep learning digital twin," in 2020 52nd North American Power Symposium (NAPS). IEEE, 2021, pp. 1-6.
- [14] P. Pileggi, J. Verriet, J. Broekhuijsen, C. van Leeuwen, W. Wijbrandi, and M. Konsman, "A digital twin for cyber-physical energy systems," in 2019 7th Workshop on Modeling and Simulation of Cyber-Physical Energy Systems (MSCPES). IEEE, 2019, pp. 1-6.
- [15] R. Snijders, P. Pileggi, J. Broekhuijsen, J. Verriet, M. Wiering, and K. Kok, "Machine learning for digital twins to predict responsiveness of cyber-physical energy systems," in 2020 8th Workshop on Modeling and Simulation of Cyber-Physical Energy Systems. IEEE, 2020, pp. 1_6
- [16] P. Moutis and O. Alizadeh-Mousavi, "Digital twin of distribution power transformer for real-time monitoring of medium voltage from low voltage measurements," *IEEE Transactions on Power Delivery*, vol. 36, no. 4, pp. 1952–1963, 2020.
- [17] A. Wunderlich and E. Santi, "Digital twin models of power electronic converters using dynamic neural networks," in 2021 IEEE Applied Power Electronics Conference and Exposition (APEC). IEEE, 2021, pp. 2369– 2376.
- [18] T. Hossen, M. Gursoy, and B. Mirafzal, "Digital twin for self-security of smart inverters," in 2021 IEEE Energy Conversion Congress and Exposition (ECCE). IEEE, 2021, pp. 713–718.
- [19] P. Jain, J. Poon, J. P. Singh, C. Spanos, S. R. Sanders, and S. K. Panda, "A digital twin approach for fault diagnosis in distributed photovoltaic systems," *IEEE Transactions on Power Electronics*, vol. 35, no. 1, pp. 940–956, 2019.
- [20] M. Milton, C. De La O, H. L. Ginn, and A. Benigni, "Controllerembeddable probabilistic real-time digital twins for power electronic converter diagnostics," *IEEE Transactions on Power Electronics*, vol. 35, no. 9, pp. 9850–9864, 2020.
- [21] R. Rosen, G. Von Wichert, G. Lo, and K. D. Bettenhausen, "About the importance of autonomy and digital twins for the future of manufacturing," *Ifac-papersonline*, vol. 48, no. 3, pp. 567–572, 2015.
- [22] L. Ribeiro and M. Björkman, "Transitioning from standard automation solutions to cyber-physical production systems: an assessment of critical conceptual and technical challenges," *IEEE systems journal*, vol. 12, no. 4, pp. 3816–3827, 2017.
- [23] E. Glaessgen and D. Stargel, "The digital twin paradigm for future NASA and US Air Force vehicles," in 53rd AIAA/ASME/ASCE/AHS/ASC structures, structural dynamics and materials conference 20th AIAA/ASME/AHS adaptive structures conference 14th AIAA, 2012, p. 1818.
- [24] E. Negri, L. Fumagalli, and M. Macchi, "A review of the roles of digital twin in CPS-based production systems," *Procedia manufacturing*, vol. 11, pp. 939–948, 2017.
- [25] J. Bickford, D. L. Van Bossuyt, P. Beery, and A. Pollman, "Operationalizing digital twins through model-based systems engineering methods," *Systems Engineering*, vol. 23, no. 6, pp. 724–750, 2020.
- [26] C. Brosinsky, X. Song, and D. Westermann, "Digital twin-concept of a continuously adaptive power system mirror," in *International ETG-Congress 2019; ETG Symposium.* VDE, 2019, pp. 1-6.